

Electronic Supplementary Information

Mechanism Study on Photocatalytic Inactivation for *Salmonella typhimurium*

Bacteria by Cu_xO loaded Rhodium-Antimony co-doped TiO₂ Nanorod

Love Kumar Dhandole^{†a}, Young-Seok Seo^{†a}, Su-Gyeong Kim^a, Aerin Kim^a, Min Cho^{*a} and

Jum Suk Jang^{*a}

^aDivision of Biotechnology, Advanced Institute of Environment and Bioscience, College of Environmental and Bioresource Sciences, Chonbuk National University, Iksan, 54596, Korea

[†] Equal contribution

*Corresponding authors. Tel.: +82 63 850 0846; fax: +82 63 850 0834.

E-mail address: jangjs75@jbnu.ac.kr (J.S. Jang) and cho317@jbnu.ac.kr (Min Cho)

Fig. S1 Field emission scanning electron microscopy images of (a) Rh-Sb-TiO₂ NR, and (b) Cu_xO/Rh-Sb-TiO₂ NR.

Fig. S2 Elemental analysis of EDAX (A and B) of (a) Rh-Sb-TiO₂ NR [1.0 M] and (b) Cu_xO (2 wt%)/Rh-Sb-TiO₂ NR [1.0 M].

Fig. S3 (A) X-ray diffraction patterns, and (B) UV-DRS spectrum, of (a) Rh-Sb-TiO₂ NR, and (b) Cu_xO/Rh-Sb-TiO₂ NR.

Fig. S4 X-ray photoelectron spectra for Cu 2p, Rh 3d, Sb 3d, and Ti 2p, of (a) Rh-Sb-TiO₂ NR, and (b) Cu_xO/Rh-Sb-TiO₂ NR photocatalyst.

Fig. S5 The high resolution Cu 2p_{1/2} and Cu 2p_{3/2} fitted XPS plot.

Fig. S6 Inactivation of *S. typhimurium* by (a) Cu_xO/Rh-Sb-TiO₂ NR in visible light condition, (b) UVC irradiation, and (c) TiO₂/UVA (21±1 °C; pH: 7.0; [Cu_xO/Rh-Sb-TiO₂ NR]₀ = [TiO₂]₀: 0.5 g/L; [N]₀: 1x10⁵ ~ 10⁶ CFU/mL; light intensity: 300 μW/cm² for (a), 0.1 mW/cm² for (b), 1.8 x 10⁻⁶ einsteinin/L·s for (c); UV cut-off filter for (a)).

Fig. S7 HCHO production (from methanol oxidation) by Cu_xO/Rh-Sb-TiO₂ NR, Rh-Sb-TiO₂ NR, and TiO₂/UVA (21±1 °C; pH: 7.0; [Cu_xO/Rh-Sb-TiO₂ NR]₀ = [Rh-Sb-TiO₂ NR]₀ = [TiO₂]₀: 0.5 g/L; [Methanol]₀: 200 mM; light intensity: 300 μW/cm², 1.8 x 10⁻⁶ einsteinin/L·s for TiO₂/UVA; UV cut-off filter for Cu_xO/Rh-Sb-TiO₂ NR and Rh-Sb-TiO₂ NR)

Fig. S8 Changes in enzymatic activity of *S. typhimurium* inactivation (1 log) by Cu_xO/Rh-Sb-TiO₂ NR in visible light condition ((a): untreated, (b): treated; 21±1 °C; pH: 7.0; [Cu_xO/Rh-Sb-TiO₂ NR]₀ = 0.5 g/L; [N]₀: 1x10⁷ CFU/mL).

Fig. S9 Photocatalytic Orange (II) dye degradation by Rh-Sb-TiO₂ NR (red line), Cu_xO/Rh-Sb-TiO₂ NR under dark (blue line) and light (black line), copper nitrate solution (added physically before light irradiation).

1.1 Morphological analysis

Scanning electron microscopy (SEM) observation was carried out by field emission scanning electron microscopy (FESEM) (SUPRA 40VP, Carl Zeiss, Germany) Chonbuk National University, equipped with X-ray energy dispersive spectrometry (EDS). Figs. S1 (a) and (b) show the FE-SEM images of without and with Cu_xO loaded Rh-Sb- TiO_2 NRs, respectively. The one-dimensional nanorod morphology was observed for both of the samples. The nanorods have a diameter in the range (80–270) nm and length of c.a. (1–2.8) μm . Our previous study has demonstrated the effect of acid treatment of rutile type TiO_2 nanorods.¹ In brief, the nanorods surface was composed of sodium ions and small nanoparticles residues. To reduce the surface irregularities, the as-prepared nanorods were HCl treated. The reduced concentration of sodium ions and concentration of copper loading were confirmed by elemental EDX analysis, and are shown in Figs. S2(a) and (b), respectively.

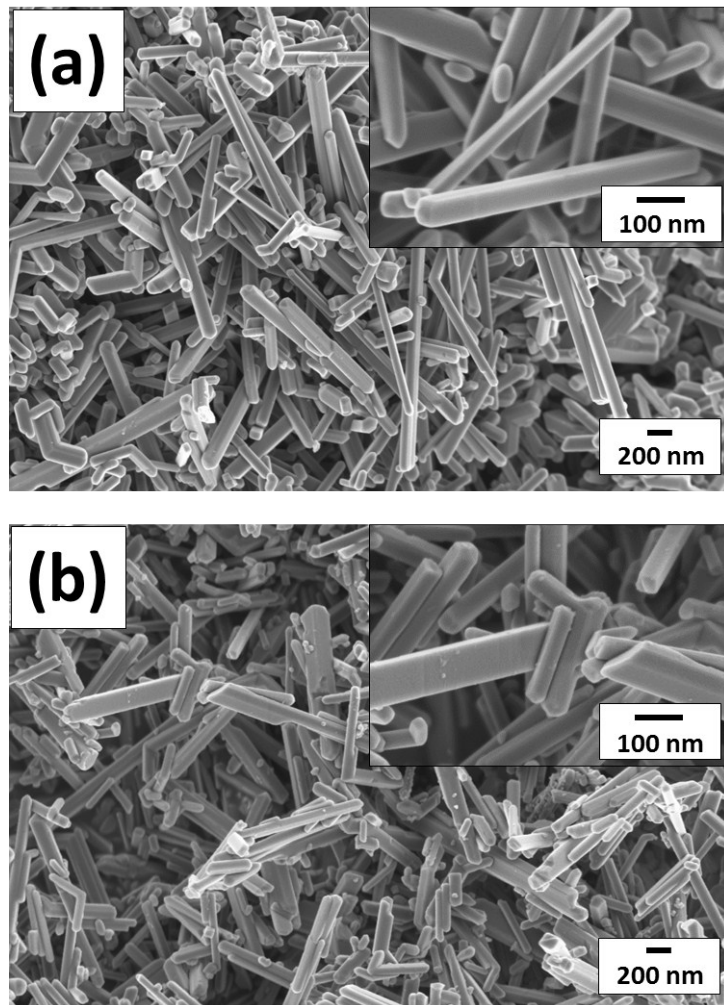
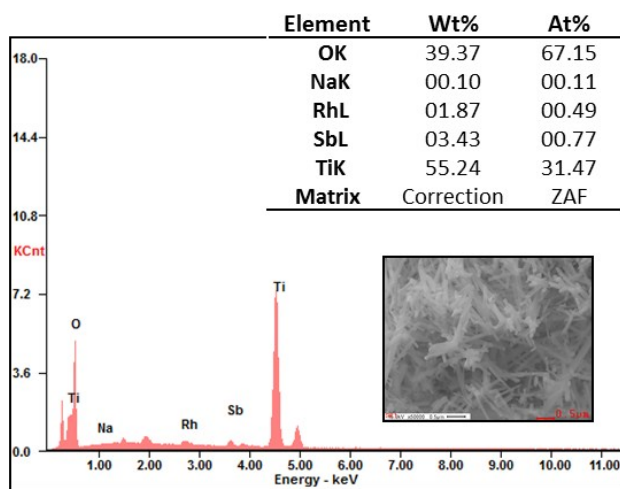


Fig. S1

(a)



(b)

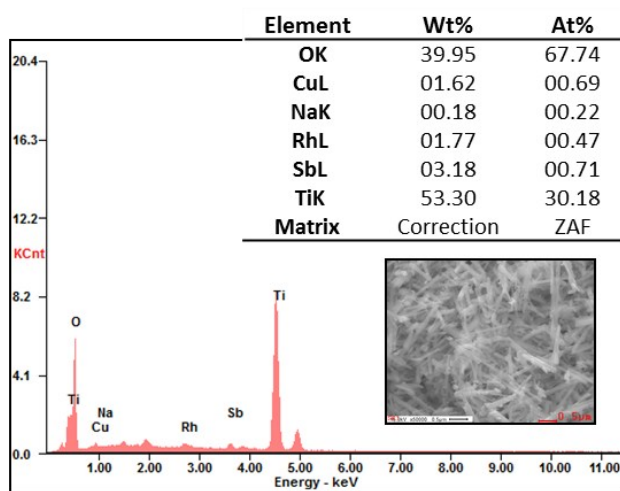


Fig. S2

1.2 Structural and optical analysis

The XRD analysis was carried out at the 5A beamline of the Pohang Light Source II (PLS-II) in Korea. The standard (θ - 2θ) scan was performed with X-ray of 11.57 keV ($\lambda=0.1072$ nm). UV-vis diffuse reflectance spectroscopy (UV-vis DRS) was obtained by Shimadzu UV-2600 UV-vis spectrophotometry. Photocatalytic experiments were performed under one sun ($1,000$ W/m²) irradiation, using solar light source (Abet Technologies Inc., USA). Fig. S3(A) shows the X-ray diffractions (XRD) patterns of the without and with Cu_xO loaded Rh-Sb-TiO₂ NRs. Major X-ray diffraction peaks at 2θ of (27.5, 36.1, and 54.4)^o correspond to (110), (101), and (211) crystal planes, respectively, and could be indexed to the tetragonal rutile phase of TiO₂ (JCPDS 89-4202).¹⁻³ Fig. S3(B) shows the UV-vis-absorption spectra of both the samples. Both samples showed the absorption band in the visible light region, with the onset of absorbance at around 630 nm. Two shoulder peaks that appeared at around (450 and 600) nm were assigned to Rh³⁺ and Rh⁴⁺, respectively.^{4,5} In comparison, the shoulder peak intensity of Cu_xO loaded Rh-Sb-TiO₂ NRs sample was decreased after Cu_xO loading (as shown in Fig. S3(B)).

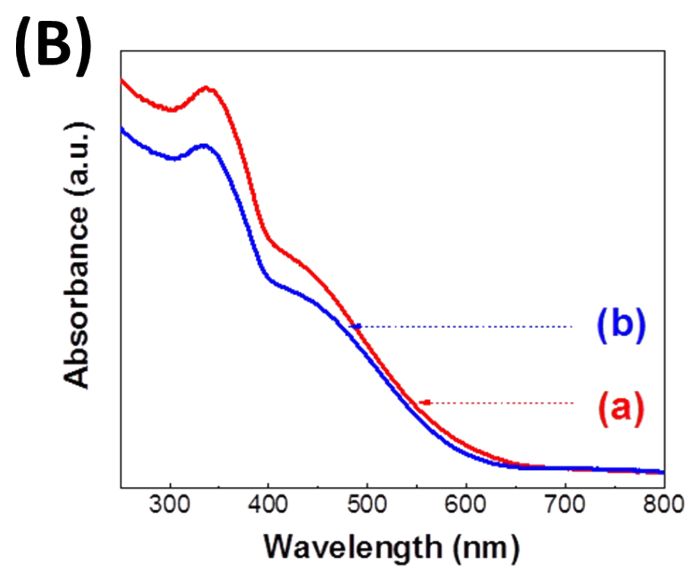
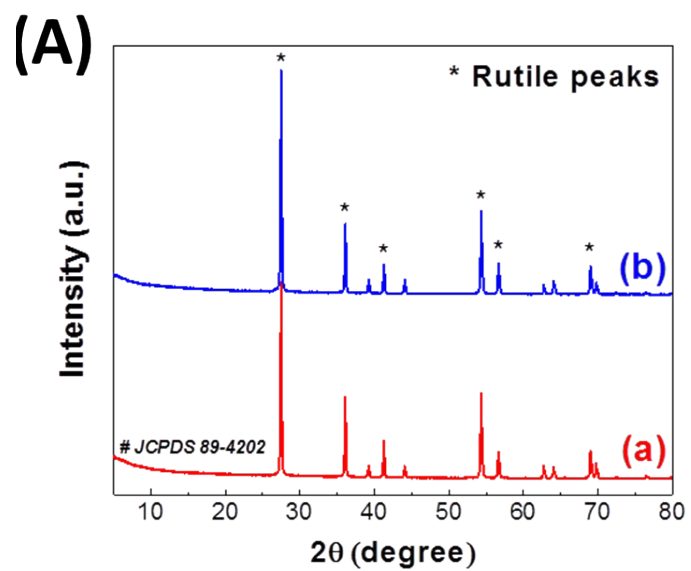


Fig. S3

1.3 Elemental analysis

X-ray photoelectron spectroscopy (XPS, Thermo Scientific XPS spectrometer) equipped with a monochromatic $A_1 K_{\alpha}$ X-ray source ($h\nu = 1,486.6$ eV) was used to study the valence state and elemental quantification of samples. X-ray photoelectron spectroscopy (XPS) elemental analysis has been performed to understand the chemical and electronic state of the copper, rhodium, antimony, and titania elements. Fig. S4 shows the high-resolution XPS spectra of Cu 2p, Rh 3d, Sb 3d, and Ti 2p. It is clear that copper is composed of doublet peaks at the two binding energies of 931.79 eV and 951.56 eV that represent Cu 2p_{3/2} and Cu 2p_{1/2} oxidation states, respectively.⁶ Fitted curve corresponding Cu peaks is shown in Fig. S5. The measured binding energy at 931.79 eV suggests the oxidation state of copper on the TiO₂ surface corresponds to Cu⁺ in Cu₂O.^{7,8} Other than these characterized main peaks, two ‘shake-up’ satellites (denoted as Sat.) peaks are located at the binding energies of 941.78 eV and 961.48 eV, respectively. The peak at 933.64 eV and shake-up peak indicate the presence of Cu²⁺ in CuO (Fig. S5).^{9,10} These peaks clearly indicate that Cu²⁺ is the dominant copper species. In both the samples, the rhodium high-resolution spectra shows doublet peaks at the binding energies of (308.84 and 313.44) eV, which are attributed to Rh 3d_{5/2} and Rh 3d_{3/2}, respectively. The appearance of spin-orbit doublet peaks of Ti at the binding energies 457.74 eV and 463.43 eV confirm that the titanium is ascribed to Ti⁴⁺ oxidation state.

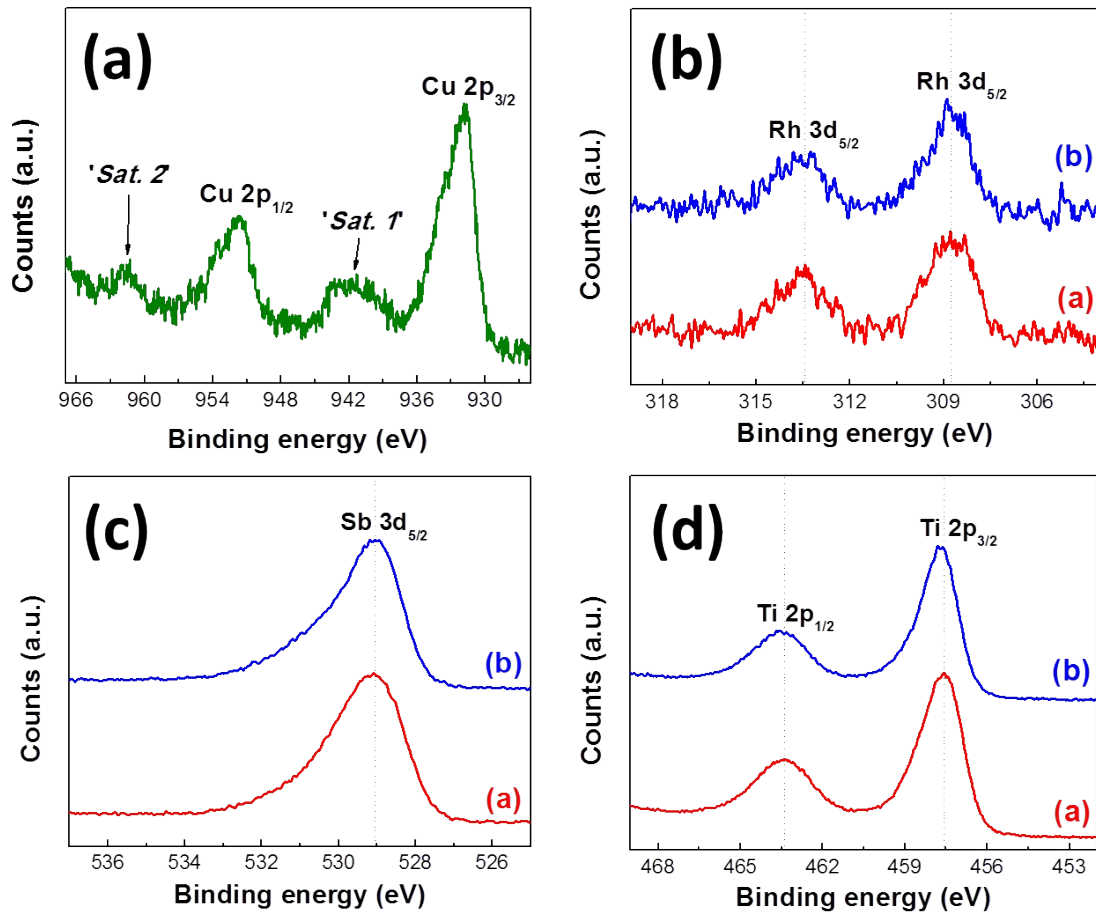


Fig. S4

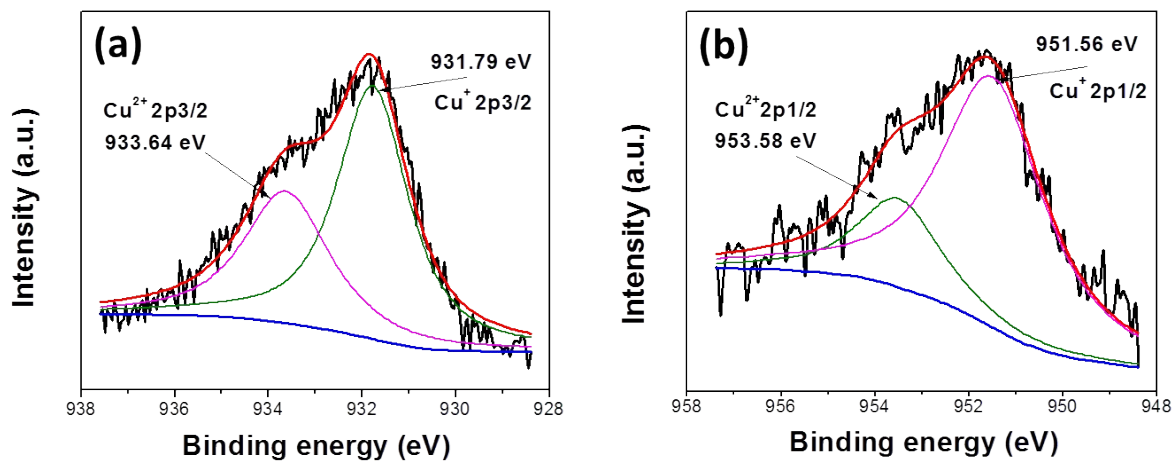


Fig. S5

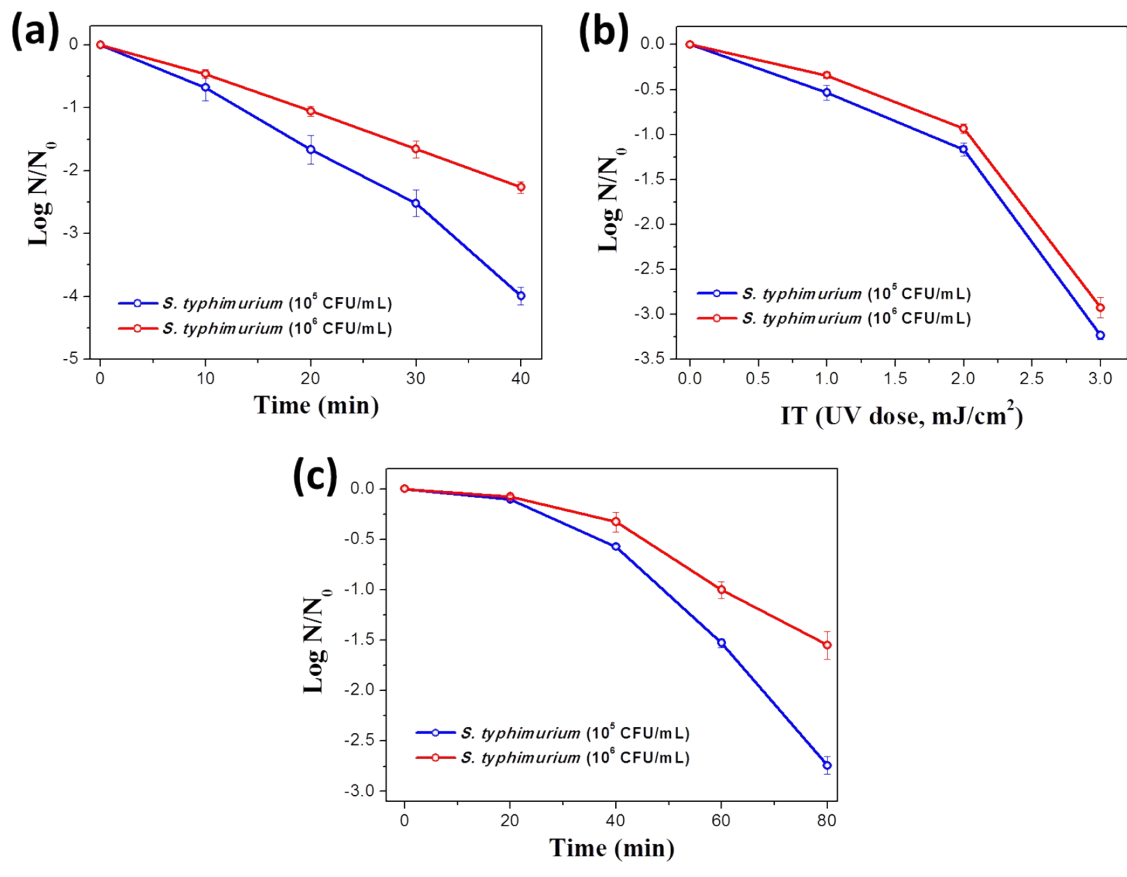


Fig. S6

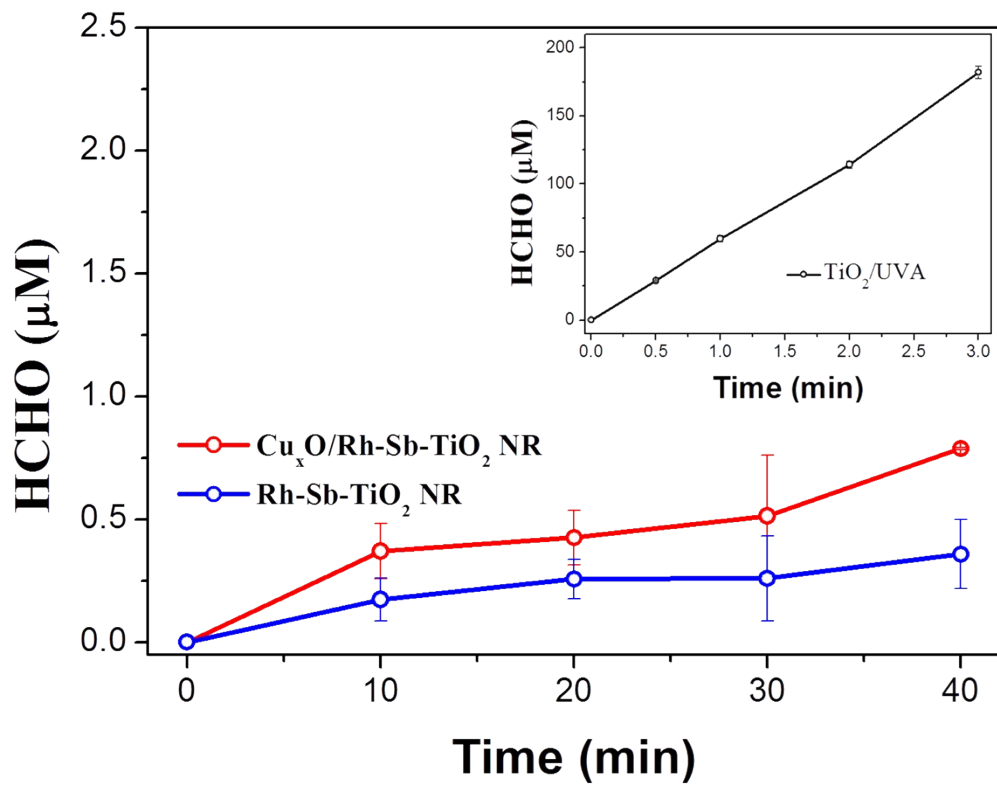


Fig. S7



Fig. S8

1.4 Degradation experiments

Closed Pyrex glass vessel was used to perform dye degradation experiment under visible light irradiation at ambient temperature. A 50 mg of as-prepared catalyst was dispersed in 45 mL of 25 μ M aqueous Orange (II) dye. Initially, the solution was stirred for 30 min in dark, to ensure good adsorption equilibrium between the catalyst and the dye solution. Catalytic reaction was initiated under visible light (420 nm cutoff filter), by using 150 W, Xenon arc lamp (Abet, Japan) for the next 5 h. The 1.4 mL of dye samples was extracted by using a syringe filter (pore size 0.2 nm) after 30 min, and later at intervals of 60 min each. UV-vis spectrophotometry (Shimadzu UV-2600 UV-vis-spectrophotometer) was used to monitor the dye degradation. Typically, during the course of reaction, the dark sampling was performed for five h, named as background test. Maximum dye absorbance wavelength (λ_{\max}) of 484 nm was used for the absorbance measurement.

Also, the dye degradation efficiency was calculated using the following Eq. (1):

$$\text{Dye degradation efficiency (\%)} = \left(1 - \frac{At}{A_0}\right) \times 100 \quad (1)$$

where, A_0 is the initial absorbance of the dye solution before the reaction, and At is the dye absorbance during the reaction at time t .

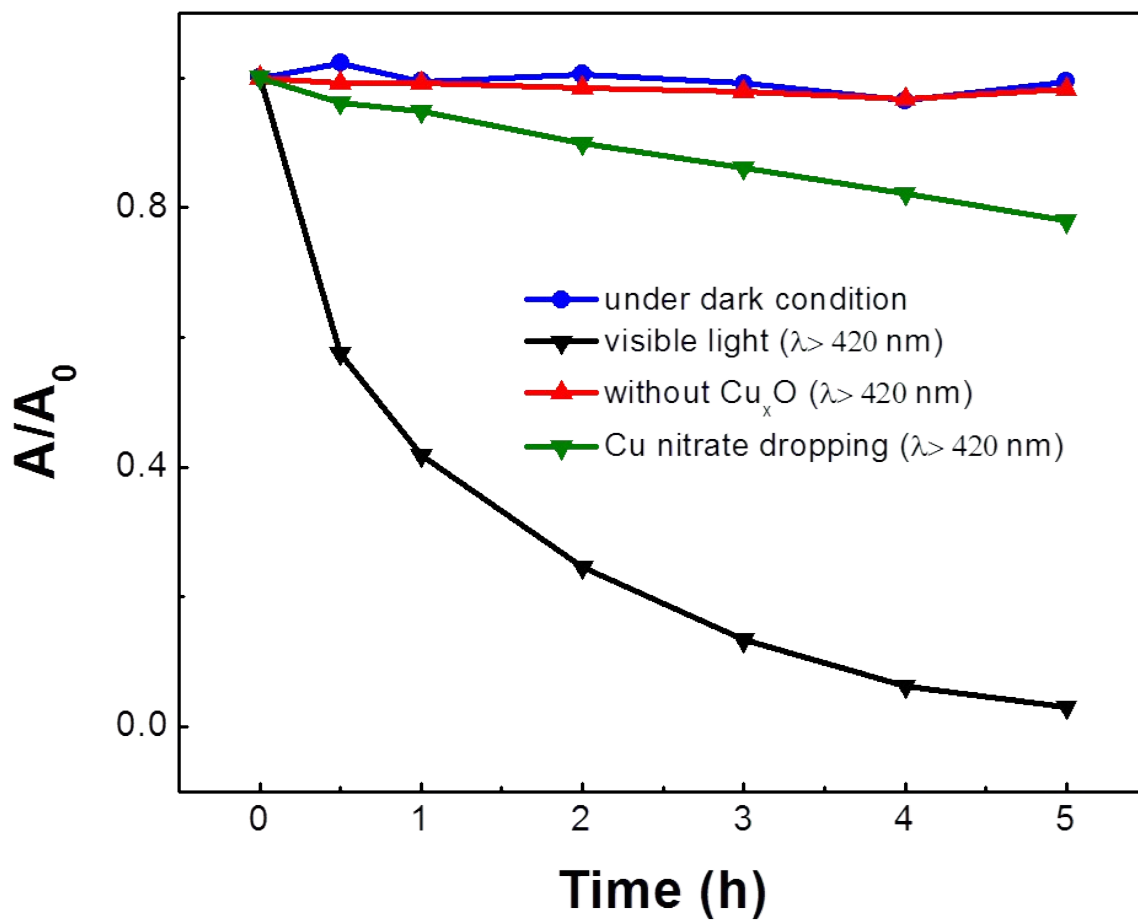


Fig. S9

References

1. L.K. Dhandole, M.A. Mahadik, S.G. Kim, H.S. Chung, Y.S. Seo, M. Cho, J. Ryu, J.S. Jang, *ACS Appl. Mater. Interfaces*, 2017, **9** (28), 23602-23613.
2. B. Liu, H.M. Chen, C. Liu, S.C. Andrews, C. Hahn, P.D. Yang, *J. Am. Chem. Soc.*, 2013, **135** (27), 9995-9998.
3. A. Fakharuddin, F. Giacomo, A.L. Palma, F. Matteocci, I. Ahmed, S. Razza, A. D'Epifanio, S. Licoccia, J. Ismail, A. Di Carlo, T.M. Brown, R. Jose, *ACS Nano*, 2015, **9** (8), 8420-8429.
4. J. Kunczewicz, B. Ohtani, *Chem. Commun.*, 2015, **51** (2), 298-301.
5. R. Niishiro, R. Konta, H. Kato, W.J. Chun, K. Asakura, A. Kudo, *J. Phys. Chem. C*, 2007, **111** (46), 17420-17426.
6. H.X. Chen, K.D. Hau, *Sci. Rep.*, 2017, **7**, 1-12.
7. K. Lalitha, G. Sadanandam, V.D. Kumari, M. Subrahmanyam, B. Sreedhar, N.Y. Hebalkar, *J. Phys. Chem. C*, 2010, **114** (50), 22181-22189.
8. Y. Wu, G. Lu, S. Li, *Catal. Lett.*, 2009, **133** (1-2), 97-105.
9. S.W. Moulder JF, P.E. Sobol, K.D. Bomben, Handbook of X-ray photoelectron spectroscopy, Perkin-Elmer Corporation 1993.
10. G. Li, N.M. Dimitrijevic, L. Chen, T. Rajh, K.A. Gray, *J. Phys. Chem. C*, 2008, **112** (48), 19040-19044.